

Constrained Bayesian Optimization Under Partial Observations: Balanced Improvements and Provable Convergence*

Shengbo Wang¹ and Ke Li²

¹College of Computer Science and Engineering, University of Electronic Science and Technology of China, Chengdu 611731, China

²Department of Computer Science, University of Exeter, EX4 4QF, Exeter, UK

*Email: shnbo.wang@foxmail.com, k.li@exeter.ac.uk

Abstract

The partially observable constrained optimization problems (POCOPs) impede data-driven optimization techniques since an infeasible solution of POCOPs can provide little information about the objective as well as the constraints. We endeavor to design an efficient and provable method for expensive POCOPs under the framework of constrained Bayesian optimization. Our method consists of two key components. Firstly, we present an improved design of the acquisition functions that introduces balanced exploration during optimization. We rigorously study the convergence properties of this design to demonstrate its effectiveness. Secondly, we propose a Gaussian process embedding different likelihoods as the surrogate model for a partially observable constraint. This model leads to a more accurate representation of the feasible regions compared to traditional classification-based models. Our proposed method is empirically studied on both synthetic and real-world problems. The results demonstrate the competitiveness of our method for solving POCOPs.

1 Introduction

The black-box constrained optimization problem considered in this paper is formulated as:

$$\text{minimize } f(\mathbf{x}) \quad \text{subject to } \vec{g}(\mathbf{x}) \leq 0, \quad (1)$$

where $\mathbf{x} = (x_1, \dots, x_n)^\top \in \Omega$ denotes the decision variable, $\Omega = [x_i^L, x_i^U]_{i=1}^n \subset \mathbb{R}^n$ denotes the search space, x_i^L and x_i^U are the lower and upper bounds of x_i respectively. The objective function $f(\mathbf{x})$ and m constraint functions $\vec{g}(\mathbf{x}) = (g_1(\mathbf{x}), \dots, g_m(\mathbf{x}))^\top$ are: *i) analytically unknown*, we do not have access to f and \vec{g} directly, but to \mathbf{x}^i to be determined and their observations $f(\mathbf{x}^i)$ and $\vec{g}(\mathbf{x}^i)$ instead; *ii) computationally expensive*, we should find a better solution in a limited budget of observations; and *iii) partially observable*, the values of f and \vec{g} can be unobservable when a candidate solution is *infeasible*. We denote the unknown feasible space by $\chi = \{\mathbf{x} \in \Omega | \vec{g}(\mathbf{x}) \leq 0\}$. Partially observable constrained optimization problems (POCOPs) are not uncommon in real-life applications. For example, a robot control task will be suspended when a collision or excessive

*This manuscript is submitted for potential publication. Reviewers can use this version in peer review.

instantaneous power consumption is detected, where the feedback is merely a failure message rather than any reward [1]. An AutoML task will be terminated without outputting the performance of a hyperparameter configuration but an error log when there is a memory overflow or computation timeout [2].

Bayesian optimization (BO) is recognized as an effective query-efficient framework for black-box optimization [3]. Although there have been dedicated efforts on constraint handling in the context of BO, a.k.a. constrained Bayesian optimization (CBO), most of them are however expected to work with complete observations. With missing values, the existing CBO methods may become inefficient due to the following two issues.

- It is more likely for a CBO method to perform an over-exploitation on the known feasible regions when solving POCOPs. As the objective values are not observable outside χ , the update of an acquisition function, such as expected improvement (EI), will be stagnated. Therefore, more observations will be clustered in local feasible regions, What is worse, this can result in an *over-confidence* in both surrogate modeling and candidate acquisition, thus reducing the optimization efficiency.
- With partial observations, conventional surrogate models lack of a sufficient exploitation upon the valid (mixed) data. A probabilistic classifier, such as the Gaussian process classifier (GPC), is utilized to identify feasible/infeasible solutions of a constraint [4]. However, an observed value cannot be used to refine a classification-targeted model. To leverage value observations, injecting artificial values to infeasible solutions enables to use regression models [5], at a risk of bringing additional incorrect priors.

Bearing these considerations in mind, this paper proposes a novel CBO framework for solving POCOPs. Our main contributions are outlined as follows.

- To mitigate the risk of an over-exploitation upon an evaluated local feasible region, we design a new acquisition function that augments the EI with a more balanced constraint handling technique. It includes an exploration function that enables to facilitate global search during optimization. [We also investigate the convergence property of this design in theory for demonstration.](#)
- To fully exploiting the mixed observations, we introduce heterogeneous-likelihood Gaussian processes (HLGPs), which leads to a better representation of unknown constraints than classifier-based models empirically. To deal with the non-Gaussian inference, we leverage the expectation propagation for Gaussian approximation of HLGPs with high computational efficiency.
- We propose an illustrative exploration function that assigns more balanced weights for potential boundaries. Moreover, we conduct experiments on different CBO methods and modeling techniques. The empirical results demonstrate that our method is a competitive CBO method for solving POCOPs in an efficient manner.

2 Related Works

2.1 Constrained Bayesian Optimization

Classic CBO methods usually reshape an unconstrained acquisition function by incorporating feasibility considerations. A prominent approach, EI with constraints (EIC), first introduced by [6], has been extensively employed to locate feasible solutions with high probability [7, 8]. To further enhance EIC’s capability in noisy environments, [9] leveraged a quasi-Monte Carlo approximation. Furthermore, various strategies such as integration [8], rollout [10], and a two-step lookahead algorithm [11], have been proposed to achieve a better optimization efficiency. These approaches increase the exploration of unknown regions, albeit at the cost of computational complexity, often hindering their scalability for high-dimensional problems.

From the perspective of uncertainty reduction, predictive entropy search (PESC), which selects feasible candidate solutions directly from the search space, offers an attractive solution to constrained optimization problems [12]. However, the intractable nature of quadrature calculations during sampling in PESC has been a challenge. To address this, [13] proposed the min-value entropy search, enabling the sampling process to operate more effectively within the objective space. This concept has subsequently been extended to accommodate binary observations [2] and multi-objective optimization problems [14]. Furthermore, the fusion of EI and entropy search has shown promise for enhancing exploration [4].

To harness the structure inherent in equation (1), researchers such as [15] and [16] proposed the utilization of a Lagrangian method with slack variables, providing the capability to deal with equality constraints. Regarding problems marked by unknown constraints, [17] have integrated BO with the alternating direction method of multipliers (ADMM), thereby enabling the exploration of solutions even in the absence of feasible ones. Meanwhile, [18] proposed the use of Thompson sampling combined with a trust region approach, aiming to enhance the scalability of CBO. This approach also incorporates a thoughtful design aimed at maintaining computational efficiency.

2.2 Surrogate Models for Constraints

The aforementioned CBO methods frequently employ Gaussian Process regression (GPR) and GPC to construct surrogate models for unknown constraints. Notably, classifiers such as GPC and support vector machine (SVM) have been found effective in sequential updates when the real value of an infringed constraint remains unobservable [2, 4, 17, 19, 20]. Yet, in partially observable scenarios, these classifiers exhibit limitations in utilizing available observations, resulting in a dip in modeling performance. In response to this challenge, [1] enhanced the construction of GPR models by introducing a switched likelihood combined with mixed data observations. As an alternative solution, [21] and [22] proposed multivariate GPs (MVGP) with joint distributions of hybrid input to handle mixed observations.

2.3 Exploration for Unknown Feasible Regions

In light of the black-box nature of the problem at hand, discerning the feasibility of a solution becomes a significant concern. In this context, [23] interpreted the delicate balance between enhancing the probability of feasibility (POF) and optimizing the objective as a multi-objective optimization issue. Focusing on optimization, [24] developed a step-wise uncertainty reduction method, which capitalizes on the volume of feasible regions beneath the most promising solution observed up to

that point, despite the method’s considerable computational complexity. Furthermore, the EIC was adapted in [4, 25] to deepen the understanding of global feasible regions. Regarding exploration, level-set and contour estimation techniques have been adapted to locate unknown feasible regions [26–28]. Yet, these methods can be excessively aggressive, thereby hindering optimization progress.

3 Preliminaries of CBO

Conventional BO starts from uniformly sampling a set of solutions according to a space-filling experimental design method. Thereafter, it sequentially updates its next sample until the given computational budget is exhausted. BO consists two main components: *i*) a surrogate model for approximating the true expensive objective function; and *ii*) an infill criterion (based on the optimization of an acquisition function) for deciding the next point of merit.

3.1 Surrogate model

Given a set of training data $\mathcal{D} = \{(\mathbf{x}^i, f(\mathbf{x}^i))\}_{i=1}^N$, we apply the GPR model to learn a latent function $\tilde{f}(\mathbf{x})$ with a prior mean function $m(\mathbf{x})$ and a noise-free likelihood [29]. For a candidate solution $\tilde{\mathbf{x}}$, the mean and variance of the target $f(\tilde{\mathbf{x}})$ can be predicted as:

$$\begin{aligned}\mu_f(\tilde{\mathbf{x}}) &= m(\tilde{\mathbf{x}}) + \mathbf{k}^{*\top} K^{-1} \mathbf{f}', \\ \sigma_f^2(\tilde{\mathbf{x}}) &= k(\tilde{\mathbf{x}}, \tilde{\mathbf{x}}) - \mathbf{k}^{*\top} K^{-1} \mathbf{k}^*,\end{aligned}\tag{2}$$

in which \mathbf{k}^* is the covariance matrix between X and $\tilde{\mathbf{x}}$, K is the covariance matrix of X , $X = (\mathbf{x}^1, \dots, \mathbf{x}^N)^\top$ and $\mathbf{f} = (f(\mathbf{x}^1) - m(\mathbf{x}^1), \dots, f(\mathbf{x}^N) - m(\mathbf{x}^N))^\top$. In this paper, we use the Matérn 5/2 as the kernel function and a trainable constant mean function for all GP models. As for the i -th constraint in (1), it will be modeled by an independent GP model $\tilde{g}_i(\tilde{\mathbf{x}})$ whose predictive mean and variance are denoted by $\mu_g^i(\tilde{\mathbf{x}})$ and $\sigma_g^i(\tilde{\mathbf{x}})$ respectively, $i = 1, \dots, m$.

3.2 Infill criterion

Instead of directly working on $\tilde{f}(\mathbf{x})$, the actual search process of BO is driven by an acquisition function that naturally strikes a balance between exploitation of the predicted optimum and exploration of model uncertainty. This paper applies the widely used expected improvement (EI) [30] to serve this purpose:

$$\text{EI}(\tilde{\mathbf{x}}|\mathcal{D}) = \sigma_f(\tilde{\mathbf{x}})(z\Phi_f(z) + \phi_f(z)),\tag{3}$$

where $z = \frac{f_{\mathcal{D}}^* - \mu_f(\tilde{\mathbf{x}})}{\sigma_f(\tilde{\mathbf{x}})}$, $f_{\mathcal{D}}^* = \min_{(\mathbf{x}, f(\mathbf{x})) \in \mathcal{D}} f(\mathbf{x})$, Φ_f and ϕ_f denote the cumulative distribution function and probability density function, respectively.

To handle unknown constraints, EIC was proposed as a product of the EI with the POF [7]:

$$\text{EIC}(\tilde{\mathbf{x}}|\mathcal{D}) = \text{EI}(\tilde{\mathbf{x}}|\mathcal{D}) \cdot \text{POF}(\tilde{\mathbf{x}}),\tag{4}$$

with

$$\text{POF}(\tilde{\mathbf{x}}) = \mathbb{P}[\tilde{g}(\tilde{\mathbf{x}}) \leq 0] = \prod_{i=1}^m \Phi_g^i(\lambda),\tag{5}$$

Algorithm 1: Pseudo code of CBOB

Input: Initial dataset $\mathcal{D} = \{\langle \mathbf{x}^i, f(\mathbf{x}^i), \vec{g}(\mathbf{x}^i) \rangle\}_{i=1}^{N_0}$, budget N , and priors of GPs
Output: The optimal feasible objective $f_{\mathcal{D}}^*$

- 1 **for** $k \leftarrow 1$ **to** N **do**
- 2 Build a GPR model for the black-box objective;
- 3 **for** $i \leftarrow 1$ **to** m **do**
- 4 \triangleright Update \mathbf{g}_i in \mathcal{D} with modified observations $\tilde{\mu}_g^i$ and $\tilde{\Sigma}_g^i$ using equation (13);
- 5 \triangleright Build an HLGp model based on \mathbf{g}_i ;
- 6 $\triangleright \mathbf{x}^k \leftarrow \arg \max_{\tilde{\mathbf{x}} \in \Omega} \text{EICB}(\tilde{\mathbf{x}}|\mathcal{D})$;
- 7 **if** \mathbf{x}^k *is feasible* **then**
- 8 $\mathcal{D} \leftarrow \mathcal{D} \cup \{\mathbf{x}^k, f(\mathbf{x}^k), \vec{g}(\mathbf{x}^k)\}$;
- 9 **else**
- 10 $\triangleright g_i^k \leftarrow +1$ for the i -th violated constraints;
- 11 $\vec{g}(\mathbf{x}^k) = (g_1^k, \dots, g_m^k)$;
- 12 $\triangleright \mathcal{D} \leftarrow \mathcal{D} \cup \{\mathbf{x}^k, \text{Null}, \vec{g}(\mathbf{x}^k)\}$;

where Φ^i denotes the cumulative distribution function of the i -th constraint based on GPR models, λ is the threshold of a feasible level and is set as a constant 0 in this paper.

4 Proposed Method

This section delineates the implementation of our proposed method, dubbed CBOB, for POCOPs. As shown in Algorithm 1, CBOB adheres to the conventional CBO procedure while introducing two unique algorithmic components (highlighted by \triangleright). The first is a framework for designing an acquisition function, which facilitates balanced exploration by effectively harnessing the surrogate models of constraints. The second is a bespoke GP model, specifically formulated to model constraints using partial observations.

4.1 A Framework for Acquisition Function Design

Under the condition of partial observations, the EI function only updates upon evaluation of a feasible solution, while the POF predominantly targets known feasible regions. This results in an overemphasis on known feasible regions by the EIC, particularly when tackling POCOPs. Inspired by [24], we posit that prioritizing search towards less explored regions can enhance exploratory capability, thus promoting more global search behaviors in a CBO method. This approach has been empirically substantiated in [4, 10, 11]. In this work, we propose a dynamic version of POF (DPOF) that incorporates an additional exploration capability, rather than prioritizing the most uncertain region indiscriminately. The DPOF function is defined as follows:

$$\text{DPOF}(\tilde{\mathbf{x}}) = \prod_{i=1}^m \text{Proj}_{[0,1]}[(\rho^i(\tilde{\mathbf{x}}) + 1)\Phi_g^i(\lambda)], \quad (6)$$

where Proj clips values outside $[0, 1]$ to the boundaries, and ρ^i denotes a general exploration function defined below.

Definition 1 (Exploration function). *A smooth function $\rho^i(\mathbf{x}) : \Omega \rightarrow [0, \bar{\rho}]$ is a valid exploration function if it is bounded by $\bar{\rho} > 0$ and $\rho^i(\tilde{\mathbf{x}}) = 0, \forall \sigma_g^i(\mathbf{x}) = 0$.*

With an exploration function ρ^i , DPOF assigns more weights to unknown regions than POF to facilitate a global search. However, to prevent excessive exploration and maintain a high probability of obtaining feasible solutions, we multiply $\Phi_g^i(\lambda)$ with ρ^i in equation (6). Alternatively, this could be viewed as introducing a dynamic constraint threshold $\lambda(\tilde{\mathbf{x}}) = \Phi_g^i{}^{-1}(\text{DPOF}(\tilde{\mathbf{x}}))$ that varies across different candidate solutions. Note that when $\rho^i \equiv 0$, DPOF simplifies to the traditional POF. Building on this, we introduce a new acquisition function, termed as EI with constraint and balance (EICB), formulated as a product of EI and DPOF:

$$\text{EICB}(\tilde{\mathbf{x}}|\mathcal{D}) = \text{EI}(\tilde{\mathbf{x}}|\mathcal{D}) \cdot \text{DPOF}(\tilde{\mathbf{x}}). \quad (7)$$

Theorem 1. *Assume that the constraint values are fully observable. Assume also that the involved GPs are non-degenerate and satisfy the no-empty-ball property [31]. Let \mathcal{D} be the collected observations with $\langle \mathbf{x}^1, f(\mathbf{x}^1) \rangle$ fixed in χ while $\{\langle \mathbf{x}^i, f(\mathbf{x}^i) \rangle\}_{i=2}^N$ are sequentially chosen by*

$$\mathbf{x}^i = \arg \max_{\tilde{\mathbf{x}} \in \Omega} \text{EICB}(\tilde{\mathbf{x}}|\mathcal{D}). \quad (8)$$

Then, as $N \rightarrow \infty$, almost surely:

1. the acquisition function $\sup_{\tilde{\mathbf{x}} \in \Omega} \text{EICB}(\tilde{\mathbf{x}}|\mathcal{D}) \rightarrow 0$;
2. the evaluated best objective $f_{\mathcal{D}}^* \rightarrow f_{\chi}^*$;

where f_{χ}^* represents the global optimum of equation (1).

The proof of Theorem 1 is sketched in the Section A of the supplementary document. This theorem suggests that the incorporation of ρ^i as designed in equation (6) does not undermine the asymptotic convergence capability of EI-based acquisition functions, such as EICB. In the following subsection, we propose an instance of the exploration function under Definition 1 that outperforms the EIC in terms of efficiently conducting global optimization for POCOPs.

4.1.1 An instance of the exploration function

In the context of the EICB framework, exploration during optimization can be facilitated by an apt design of ρ^i . In this paper, we concentrate on identifying promising constraint boundaries, as opposed to aggressively targeting the most uncertain regions, a tactic often employed in level-set estimation and active learning [26–28, 32]. To this end, we first define a utility function representing the potential of being the boundary (POB) for the i -th constraint at $\tilde{\mathbf{x}} \in \Omega$ as follows:

$$\text{POB}^i(\tilde{\mathbf{x}}) = \begin{cases} 1, & \tilde{g}_i(\tilde{\mathbf{x}}) \in [-\varepsilon(\tilde{\mathbf{x}}), \varepsilon(\tilde{\mathbf{x}})], \\ 0, & \text{otherwise,} \end{cases} \quad (9)$$

where $\varepsilon(\tilde{\mathbf{x}}) = \beta \sigma_g^i(\tilde{\mathbf{x}})$ and $\beta > 0$ represents a confidence level. Taking the expectation of equation (9) over the predicted distribution of $\tilde{g}_i(\tilde{\mathbf{x}})$ and defining $\bar{g}_i(\tilde{\mathbf{x}}) = \mu_g^i(\tilde{\mathbf{x}})/\sigma_g^i(\tilde{\mathbf{x}})$, we obtain a valid exploration function as:

$$\rho^i(\tilde{\mathbf{x}}) = \Phi(\beta - \bar{g}_i(\tilde{\mathbf{x}})) - \Phi(-\beta - \bar{g}_i(\tilde{\mathbf{x}})), \quad (10)$$

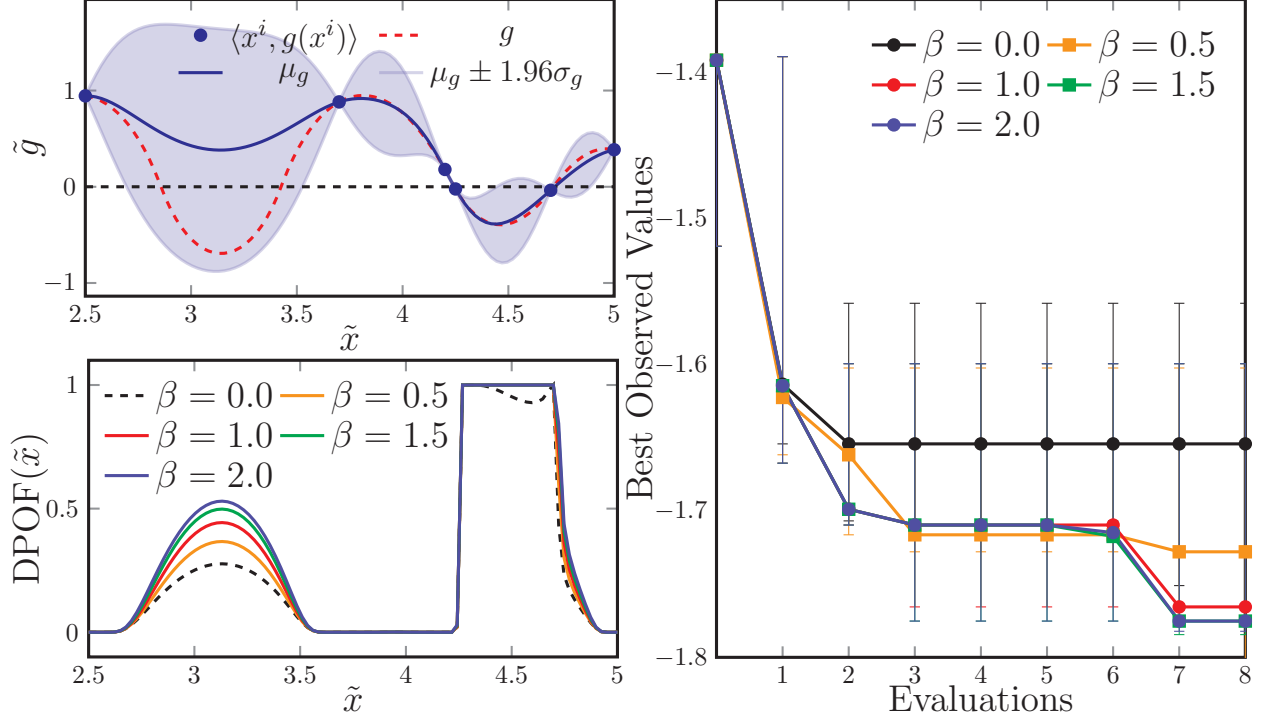


Figure 1: Illustration of EICB with equation (10) by a toy 1-D example (please refer to Section B of the supplementary document for more details). (Left up) The constraint surrogate model with 6 observed data pairs where the red dotted line denotes the true function. (Left down) The DPOF with different β on $[2.5, 5]$, where the dotted line with $\beta = 0$ reduces to POF. (Right) Optimization trajectories on $[0, 10]$ with 5 randomly repeated experiments.

where Φ is the cumulative distribution function of $\mathcal{N}(0, 1)$.

The illustrative example in Figure 1 demonstrates how DPOF, given a surrogate model for a constraint, assigns more weight to the unknown feasible region ($[2.85, 3.45]$ in this case) as β increases. For a previously located feasible region such as $[4.3, 4.7]$, DPOF provides equal weights (approximately 1) to all candidates within this region when $\beta \geq 0.5$. In contrast, POF ($\beta = 0$) assigns differentiated weights based on different $\Phi_g(0)$ values. By refining the boundary, DPOF ensures a more balanced weight distribution within the located feasible region, hence the nomenclature, EICB. We posit that this balanced approach enhances the decision-making capabilities of EI, as compared to the imbalanced weights scenario posed by POF. As a positive consequence, EICB encourages greater exploration towards unknown regions. As ρ^i in equation (10) is bound by 1, DPOF can assign a maximum of $2\Phi_g(0)$ to any given candidate. Empirically, this subtle adjustment leads to enhanced optimization efficiency as evidenced in Figure 1, thanks to the introduction of exploration. Besides, we provide a more aggressive design of ρ^i that bolsters the reduction of uncertainty in global feasible regions. Due to the space restriction, this discussion is presented in Section B of the supplementary document.

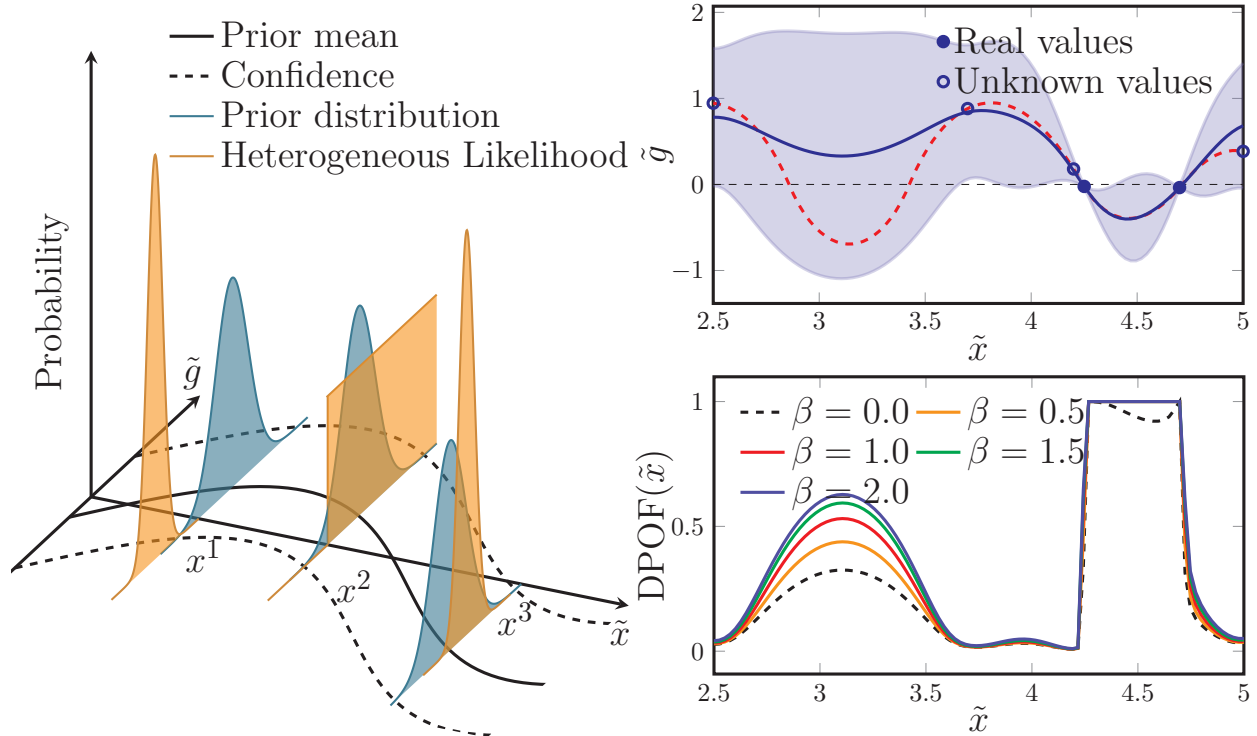


Figure 2: Illustration of HLGPs. (Left) Three observations with heterogeneous likelihood distributions, including a truncated distribution on x^2 , and Gaussian distributions on x^1 and x^3 . (Right up) An EP-based HLGPs model with partial observations. (Right down) The DPOF with different β .

4.2 Surrogate Models Under Partial Observations

When dealing with partially observable constraints, observations are composed of two distinct aspects: *i*) the actual values associated with feasible solutions, and *ii*) the truncated distribution of possible values for all solutions, such as $\mathbb{P}(\tilde{g} > 0) = 1$, as depicted in Figure 2. The simultaneous consideration of these two types of observations can be achieved by attaching individual likelihood distributions to feasible/infeasible solutions, as is done in HLGPs.

For the i -th constraint, the posterior of a latent function, $p(\tilde{\mathbf{g}}_i | X, \mathbf{g}_i)$, within an HLGPs model is determined via the Bayes rule using the prior distribution $p(\tilde{\mathbf{g}}_i | X) = \mathcal{N}(\mathbf{0}, K)$ in equation (2), along with the individual likelihood distributions. Specifically, the posterior is expressed as:

$$p(g_i^k | \tilde{g}_i^k) = \begin{cases} \mathcal{N}(g_i(\mathbf{x}^k), \sigma^2), & \text{if } g_i(\mathbf{x}^k) \leq 0, \\ \Phi(\alpha^{-1} g_i(\mathbf{x}^k)), & \text{if } g_i(\mathbf{x}^k) > 0, \end{cases} \quad (11)$$

where $k \in \{1, \dots, N\}$, $\mathbf{g}_i = (g_i^1, \dots, g_i^N)^\top$ represents N observations of $g_i(X)$, $\tilde{\mathbf{g}}_i = (\tilde{g}_i^1, \dots, \tilde{g}_i^N)^\top$ denotes N latent functions, $\sigma \geq 0$ stands for the noise level, and $\alpha > 0$ is a scaling parameter. We set $\sigma = 10^{-6}$ to indicate a noise-free environment and $\alpha = 10^{-6}$ to approximate the truncating step function that implies $\mathbb{P}(g_i(\mathbf{x}^k) > 0) = 1, \forall g_i(\mathbf{x}^k) > 0$ [33].

4.2.1 HLGP Inference via Expectation Propagation

In this paper, we employ expectation propagation (EP) [34], a principled and highly efficient approach to handle non-Gaussian likelihoods. This provides Gaussian approximations to both the posterior and predicted distributions of HLGP. First, the posterior is formulated as:

$$p(\tilde{\mathbf{g}}_i|X, \mathbf{g}_i) = \frac{1}{Z} p(\tilde{\mathbf{g}}_i|X) \prod_{k=1}^N p(g_i^k|\tilde{g}_i^k), \quad (12)$$

where Z is the normalization factor. For the k -th observation g_i^k , EP assigns it an un-normalized Gaussian distribution $t_i^k \triangleq \tilde{Z}_i^k \mathcal{N}(\tilde{\mu}_i^k, \tilde{\sigma}_i^{k,2})$ to locally approximate its exact likelihood. In this vein, the posterior is approximated by:

$$p(\tilde{\mathbf{g}}_i|X, \mathbf{g}_i) \approx \frac{1}{Z_{\text{EP}}} p(\tilde{\mathbf{g}}_i|X) \prod_{k=1}^N t_i^k = \mathcal{N}(\boldsymbol{\mu}_g^i, \Sigma_g^i) \\ \text{with } \boldsymbol{\mu}_g^i = \Sigma_g^i \tilde{\Sigma}_g^i{}^{-1} \tilde{\boldsymbol{\mu}}_g^i \text{ and } \Sigma_g^i = (K + \tilde{\Sigma}_g^i{}^{-1})^{-1}, \quad (13)$$

where $\tilde{\boldsymbol{\mu}}_g^i = (\tilde{\mu}_i^1, \dots, \tilde{\mu}_i^N)^\top$, $\tilde{\Sigma}_g^i$ denotes a diagonal matrix with the k -th element being $\tilde{\sigma}_i^{k,2}$, and Z_{EP} is the marginal likelihood. The site parameters in t_i^k of a Gaussian likelihood in equation (11) are valued by $\tilde{Z}_i^k = 1$, $\tilde{\mu}_i^k = g_i(\mathbf{x}^k)$, $\tilde{\sigma}_i^k = \sigma$. Differently, the site parameters of a non-Gaussian likelihood in equation (11) should be computed by the moment match [33]. The detailed formulations of this part are delineated in Section C of the supplementary document. For a candidate solution $\tilde{\mathbf{x}}$, the mean and variance of the HLGP model $\tilde{g}_i(\tilde{\mathbf{x}})$ are predicted as:

$$\boldsymbol{\mu}_g^i(\tilde{\mathbf{x}}) = m(\tilde{\mathbf{x}}) + \mathbf{k}^{*\top} (K + \tilde{\Sigma}_g^i)^{-1} \tilde{\boldsymbol{\mu}}_g^i, \quad (14) \\ \sigma_g^{i,2}(\tilde{\mathbf{x}}) = k(\tilde{\mathbf{x}}, \tilde{\mathbf{x}}) - \mathbf{k}^{*\top} (K + \tilde{\Sigma}_g^i)^{-1} \mathbf{k}^*.$$

In principle, the hyperparameters of EP-based GP models should be updated by maximizing the marginal likelihood Z_{EP} . Since (14) resembles (2), from another perspective, EP algorithm serves as a data generator for HLGP, i.e., assigning *virtual observations* for infeasible solutions with an estimation of noise levels. Accordingly, the hyperparameters of an HLGP model can be optimized by maximizing the marginal likelihood of a vanilla GPR model using these injected observations rather than Z_{EP} for better computation efficiency, as noted in [29].

4.2.2 Comparison with GPC

Finally, we present a brief comparison between the HLGP models in our proposed method and the GPC models frequently used in existing CBO algorithms for unobservable constraints. Notably, executing CBO routines is also feasible by only considering the truncated value distribution in equation (11). We contend that HLGP, by leveraging available observations, constructs a more reliable surrogate model than GPC. As illustrated in Figure 3, 36 equidistant solutions are evaluated, with constraint values being unobservable for half. The true boundary and the predictions made by HLGP and GPC are provided for performance assessment. The GPC model delineates the boundary by maximizing the distance between the nearest distinct solutions, mirroring the approach of a SVM [29]. This results in the prediction of three disconnected feasible regions, deviating from the true feasible region. In contrast, HLGP predicts a connected feasible region that covers the majority of the true one. As such, we anticipate that HLGP, with its superior modeling capability, can enhance optimization processes for POCOPs.

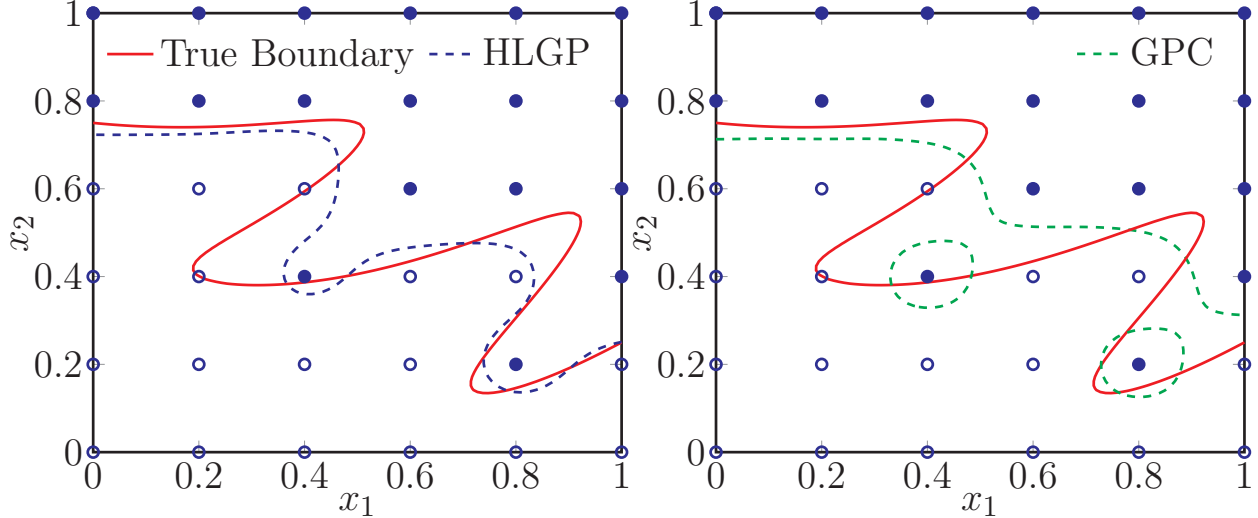


Figure 3: Different curves of feasible boundary predicted by (Left) an HLGP model versus (Right) a GPC model.

4.3 Summary of the CBOB Algorithm

To improve the optimization efficiency for POCOPs, CBOB fully exploits available observations by re-designing a more balanced acquisition function and constructing principled surrogate models from mixed observations. Our method combines a boundary-based exploration function, as in equation (10), and non-informative likelihoods as in equation (11). Moreover, CBOB preserves ample flexibility in designing exploration functions and likelihoods, thus making it adaptable to individual optimization problems and suitable for further investigations.

- Building on the concept of exploring potentially feasible regions as [4, 25], CBOB introduces extra exploration during optimization but with robust theoretical support underpinning this design. Moreover, our EICB maintains the computational efficiency of the original EIC, unlike the methods proposed in [8, 10, 11].
- Inspired by the level-set estimation methods [28], we propose an innovative exploration function that emphasizes potential boundaries for optimization, which is then further integrated with the POF in equation (6). This approach avoids the aggressive evaluation of unknown regions, which is a common tactic in [26, 27, 32].
- By employing HLGP, we build a better surrogate model for each partially observable constraint function, outperforming GPC-based methods [2, 4, 17, 19, 20]. With the aid of EP and its generated virtual observations, we manage to construct HLGP models with commendable computational efficiency, resulting in an improvement over other models with mixed observations [21, 22].

5 Experiment Setup

In this section, we present the experimental settings used in our empirical study.

5.1 Benchmark Suite

Our experiments consider various optimization tasks, including synthetic problems, engineering design cases, hyperparameter optimization (HPO) problems based on scikit-learn¹, and reinforcement learning tasks based on Open AI Gym², to constitute our benchmark suite. In addition, we consider the following two scenarios of POCOPs.

- **S1**: The first scenario is that only f is partially observable. Specifically, problems include 10D Keane’s bump function (KBF) [35], 4D welded beam design (WBD) [36], 7D HPO of XGBoost on the California housing dataset with a model size constraint (XGB-H), and 12D Lunar Landing with an energy constraint (Lunar) [37].
- **S2**: The second scenario considers both f and \vec{g} are partially observable. Specifically, problems include 10D Ackley function with one constraint (Ackley) [1], 4D pressure vessel design (PVD) [38], 8D HPO of MLP on the digits dataset with a model size constraint (MLP-D), and 16D Swimmer with an energy constraint (Swimmer) [39].

5.2 Peer Algorithms

We consider three state-of-the-art CBO methods, including EIC [7] in the EI-based family, min-value entropy search with constraints (MESc) [13] in the information-theoretic family, and Thompson sampling with constraints (TSC) [18] in the stochastic sampling family. For S2, note that both EIC and MESc can handle binary constraint feedback [2,19]. For S1, all algorithms use GPR to build the surrogate models. For S2, we choose either HLGP or GPC for modeling constraints. In particular, we use a dedicated subscript to represent the corresponding surrogate model, e.g., EIC_c and EIC_h denote EIC with GPC and HLGP, respectively.

5.3 General Settings

All algorithms are implemented based on GPflowOpt³ according to their open-source code [13,18]. In MESc, the optimal solutions are sampled 20 times. Both MESc and TSC sample with a grid size of 1000. For CBOB with equation (10), we fix $\beta = 1.96$ to obtain a 95% confidence level. As equation (10) is a conservative design for exploration, we omit the study on more conservative behaviors with smaller β .

Each experiment is independently repeated 20 times with shared random seeds. For all tasks, the Sobol sequence is used to generate $11 \times n$ initial samples, then 100 function evaluations (FEs) are performed in each experiment. Detailed settings of all algorithms and benchmark problems are presented in Section D of the supplemental document.

6 Experiment Results

The optimization trajectories of all experiments are given in Figures 4 and 5. In addition, the median best evaluated values (BOVs) and average ratios of feasible evaluations (ROFs) of different algorithms are presented in Tables 1 and 2. We empirically study the efficacy of CBOB from three

¹<https://scikit-learn.org/stable/>

²<https://gymnasium.farama.org>

³<https://github.com/GPflow/GPflowOpt>

Algorithm		KBF	WBD	XGB-H	Lunar
EIC	BOV	-0.33	2.47	0.281	255
	ROF	99.3%	75.3%	<u>22.4%</u>	82.3%
MESC	BOV	-0.29	2.28	0.271	255
	ROF	99.5%	<u>18.3%</u>	58.1%	84.5%
TSC	BOV	-0.26	2.47	0.283	247
	ROF	99.8%	77.9%	51.2%	87.7%
CBOB	BOV	-0.39	2.16	0.274	260
	ROF	<u>99.2%</u>	67.4%	25.8%	<u>70.0%</u>

Table 1: The BOV and ROF of different algorithms in S1.

aspects: *i*) the *improvement* of CBOB for EI-based CBO methods and GPC-based models; *ii*) the *competitiveness* of CBOB with other peer algorithms; and *iii*) the *relationship* between efficiency and exploration ability of CBOB.

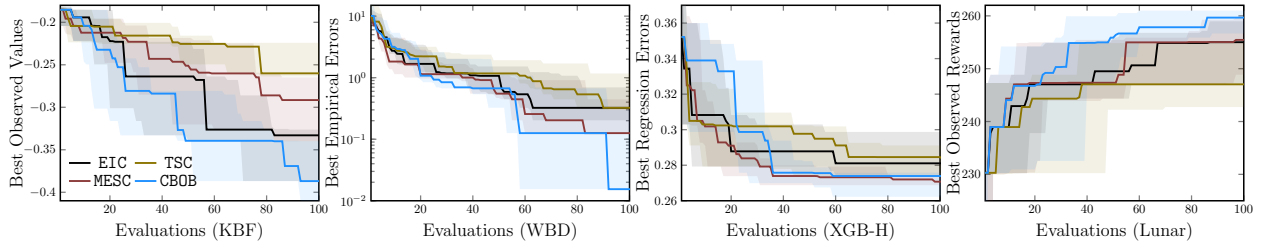


Figure 4: Optimization trajectories of different tasks in S1 (f is partially observable).

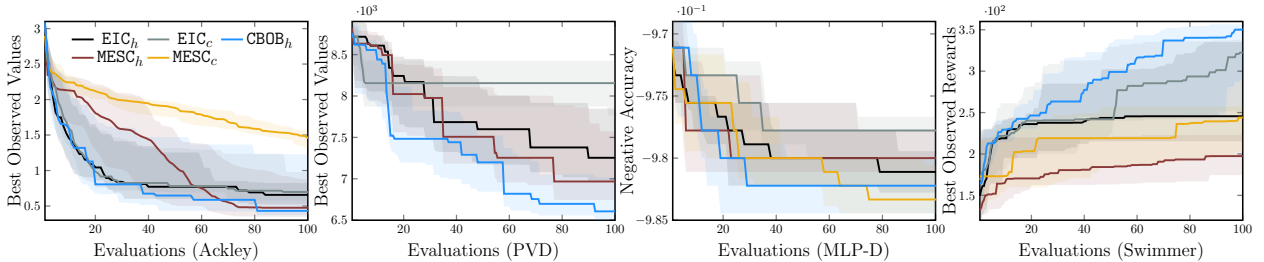


Figure 5: Optimization trajectories of different tasks in S2 (both f and \vec{g} are partially observable).

6.0.1 Improvement

Although EIC can be more efficient within 10 to 20 FEs, such as in WBD, XGB-H, Ackley and MLP-D, EICB outperforms EIC in all experiments after 100 FEs, which demonstrates the design of DPOF. As the natural expense of exploration, the value deviation of EICB may be larger during search. As given in Figure 6, despite EIC_c and EIC_h have smaller deviations of the best evaluated values, EICB obtains a more promising result in a statistical sense. In addition, compared to GPC, HLGP does not always improve EIC and MESC, whereas benefiting CBOB well.

Algorithm		Ackley	PVD	MLP-D	Swimmer
EIC _c	BOV	0.70	8155	0.978	322
	ROF	77.9%	5.12%	84.5%	82.3%
MES _c	BOV	1.44	N/A	0.983	244
	ROF	78.2%	N/A	83.1%	83.5%
EIC _h	BOV	0.66	7598	0.981	245
	ROF	38.4%	3.13%	64.8%	67.2%
MES _h	BOV	0.48	7507	0.98	197
	ROF	54.1%	3.78%	50.1%	79.8%
CBOB	BOV	0.43	7198	0.982	350
	ROF	38.0%	3.32%	65.5%	77.1%

Table 2: The BOV and ROF of different algorithms in S2.

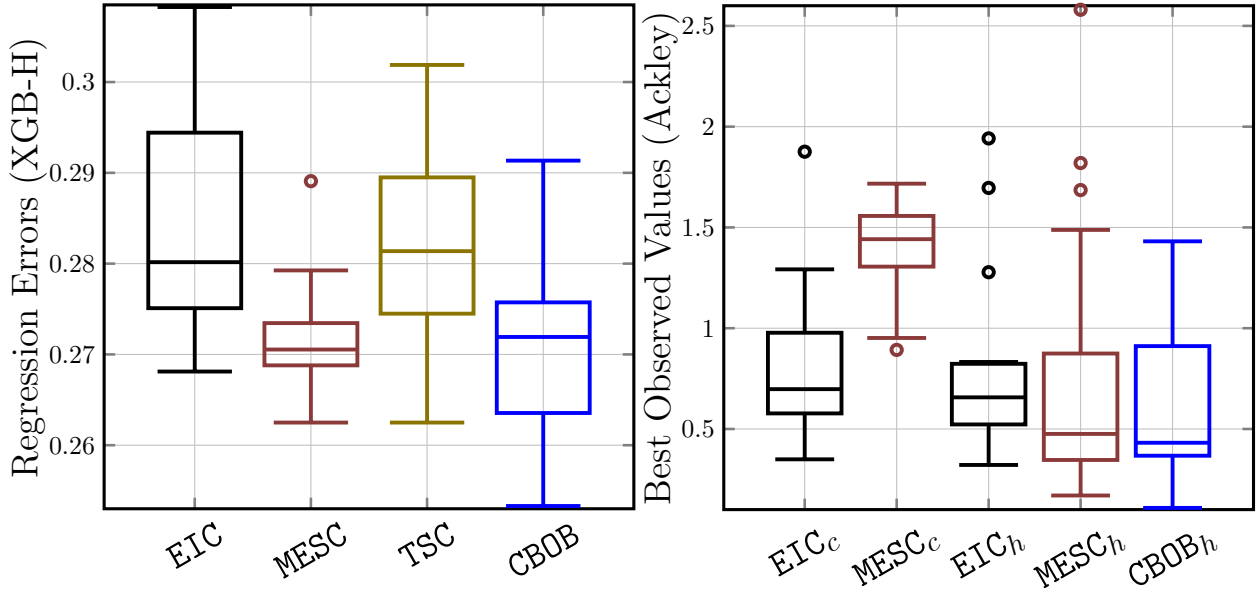


Figure 6: Box plot of the final best observed values of different algorithms on Ackley and XGB-H.

6.0.2 Competitiveness

The CBOB shows a strong competitiveness in all experiments against other CBO methods. In addition to the problems that EI-based methods perform well, such as KBF and Swimmer, CBOB remains competitive in problems that EI-based methods struggle, such as XGB-H, PVD and MLP-D. In comparison, MES_c, as a promising CBO method in most problems, is inefficient in problems such as KBF and Swimmer. The TSC that showed high efficiency in fully observable environments with trust regions [18], struggles in solving POCOPs. Moreover, CBOB and other EI-based CBO methods show less efficiency in HPO problems, which agrees with the empirical results in [40].

6.0.3 Relationship between efficiency and exploration

In Tables 1 and 2, while CBOB obtains better feasible solutions, its ROFs are relatively low, i.e., more evaluated solutions of CBOB are infeasible. On the one hand, this agrees with the ideas of [11] that exploration towards infeasible regions facilitates optimization efficiency of CBO methods. It

also explains the larger deviation of CBOB in Figure 6 that infeasible evaluations returns little information in POCOPs. Besides, we find this exploration effective as the number of outliers of CBOB reduces, such as MESC_h and CBOB in Ackley of Figure 6. On the other hand, since EI has already considered exploration, EIC can also have less ROFs during search. Differently, in order not to break the balance of EI between exploration and exploitation, CBOB assigns more balanced weights for constraint handling. We highlight that this idea can also be integrated with other acquisition functions, such as the probability of improvement and parzen estimator [3].

7 Concluding Remarks

This paper designs CBOB that fully exploits the available observations for better exploration and surrogate modeling, by both theoretical and empirical analysis, demonstrating that CBOB is potential to be a promising CBO method for POCOPs. Due to the space restriction, we provide some further discussions on the limitations and potential impact of this work in Section E of the supplementary document. Further investigations include the in-depth theoretical study of CBOB and the design of the exploration functions that are suitable for individual problems.

Acknowledgment

This work was supported by UKRI Future Leaders Fellowship (MR/S017062/1, MR/X011135/1), NSFC (62076056), EPSRC (2404317), Royal Society (IES/R2/212077) and Amazon Research Award.

Appendix Section A. Theoretical analysis of EICB

We justify the design of EICB by studying its convergence property under the framework of the *consistency* research for EI [41] and vanilla EIC [19]. In the context of sequential design, let \mathcal{F}_N denote the σ -algebra generated by the random variables $\mathbf{x}^1, Z^1, \dots, \mathbf{x}^N, Z^N$ where Z^i is the union observation of $\langle f(\mathbf{x}^i), \tilde{g}(\mathbf{x}^i) \rangle$. Additionally, let $\mathcal{F}_{N, \tilde{\mathbf{x}}}$ be the σ -algebra generated by $\mathbf{x}^1, Z^1, \dots, \mathbf{x}^N, Z^N, \tilde{\mathbf{x}}, \tilde{Z}$ with \tilde{Z} the union observation of $\langle f(\tilde{\mathbf{x}}), \tilde{g}(\tilde{\mathbf{x}}) \rangle$. Then, a sequential design strategy derived from the EICB acquisition framework takes the following form:

$$\mathbf{x}_{N+1} = \arg \max_{\tilde{\mathbf{x}} \in \Omega} \mathbb{E}_N \left[M_N^0 - M_{N, \tilde{\mathbf{x}}}^\rho \right], \quad (\text{A.1})$$

in which

$$M_{N, \tilde{\mathbf{x}}}^\rho = \min_{\mathbf{x} \in \Omega, \mathbb{P}(\tilde{g}(\mathbf{x}) < \lambda(\mathbf{x}) | \mathcal{F}_{N, \tilde{\mathbf{x}}}) = 1, \sigma_f(\mathbf{x} | \mathcal{F}_{N, \tilde{\mathbf{x}}}) = 0} \tilde{f}(\mathbf{x}), \quad (\text{A.2})$$

$$M_N^0 = \min_{\mathbf{x} \in \Omega, \mathbb{P}(\tilde{g}(\mathbf{x}) < 0 | \mathcal{F}) = 1, \sigma_f(\mathbf{x} | \mathcal{F}_N) = 0} \tilde{f}(\mathbf{x}). \quad (\text{A.3})$$

Definition 2 (Non-degenerate GPs [42]). *A GP model for $\tilde{f}(\mathbf{x})$ is non-degenerate when $\sigma_f(\mathbf{x}) = 0$ if and only if $\langle \mathbf{x}, f(\mathbf{x}) \rangle \in \mathcal{D}$.*

Definition 3 (No-empty-ball [31]). *Let $(\mathbf{x}^N)_{N \geq 1}$ be any sequence in Ω , and z be any solution in Ω . A GP model has the no-empty-ball (NEB) property, if the prediction error at z goes to zero, $\forall \epsilon > 0$, there always exists $N \geq 1$ such that $|z - \mathbf{x}^N| < \epsilon$.*

Proof of Theorem 1. When GPs are non-degenerate, equation (A.1) becomes equivalent to equation (8). Specifically, M_N^0 will be equal to f_D^* in equation (3), while $M_{N,\tilde{\mathbf{x}}}^\rho$ will be the predicted feasible objective value under dynamic constraint threshold implicitly defined by equation (6). Next, we present the criteria for *asymptotic convergence* of EICB.

The proof of the first statement, i.e., the convergence of EICB, consists of three steps.

Step 1. EICB serves as a stepwise uncertainty reduction (SUR) sequential design. For $N \geq 2$, a minimization version of equation (A.1) can be given as

$$\mathbf{x}_{N+1} = \arg \min_{\tilde{\mathbf{x}} \in \Omega} \mathbb{E}_N [H_{N,\tilde{\mathbf{x}}}], \quad (\text{A.4})$$

in which

$$\begin{aligned} H_{N,\tilde{\mathbf{x}}} &= M_{N,\tilde{\mathbf{x}}}^\rho - M_N^0 \\ &= \mathbb{E}_{N,\tilde{\mathbf{x}}} \left[M_{N,\tilde{\mathbf{x}}}^\rho - \min_{\mathbf{x} \in \Omega, \tilde{g}(\mathbf{x}) < 0} \tilde{f}(\mathbf{x}) \right]. \end{aligned} \quad (\text{A.5})$$

The above equation holds since: *i*) M_N^0 is independent from $\tilde{\mathbf{x}}$, and *ii*) $\mathbb{E}_{N,\tilde{\mathbf{x}}} [M_{N,\tilde{\mathbf{x}}}^\rho] = M_{N,\tilde{\mathbf{x}}}^\rho$ for minimum operation. Therefore EICB is transformed into a SUR sequential design for $H_{N,\tilde{\mathbf{x}}}$. Likewise, we can define

$$H_N = \mathbb{E}_N \left[M_N^\rho - \min_{\mathbf{x} \in \Omega, \tilde{g}(\mathbf{x}) < 0} \tilde{f}(\mathbf{x}) \right]. \quad (\text{A.6})$$

Step 2. (H_N) is a supermartingale. For well-structured GP models and well-defined smooth functions ρ^i , we have: *i*) $\sigma_f(\mathbf{x}|\mathcal{F}_{N+1}) \leq \sigma_f(\mathbf{x}|\mathcal{F}_N)$ (based on the definition of GP predicted variance), and *ii*) $\mathbb{P}(\tilde{g}(\mathbf{x}) < \lambda(\mathbf{x})|\mathcal{F}_N) = 1$ is sufficient for $\mathbb{P}(\tilde{g}(\mathbf{x}) < \lambda(\mathbf{x})|\mathcal{F}_{N+1}) = 1$ (based on the non-increasing property of ρ^i on an evaluated solution \mathbf{x}^N). Therefore, the following inequality holds:

$$H_N - \mathbb{E}_N [H_{N+1}] = \mathbb{E}_N [M_N^\rho - M_{N+1}^\rho] \geq 0, \quad (\text{A.7})$$

which implies that $(H_N)_{N \in \mathbb{N}}$ is a supermartingale. According to [19], there is $H_N - \mathbb{E}_N [H_{N+1}] \rightarrow 0$ as $N \rightarrow \infty$, and also

$$\sup_{\tilde{\mathbf{x}} \in \Omega} [H_N - \mathbb{E}_N [H_{N,\tilde{\mathbf{x}}}]] \rightarrow 0. \quad (\text{A.8})$$

Step 3. EICB($\tilde{\mathbf{x}}|\mathcal{D}$) converges to 0 almost surely. Note that for N observed solutions, $M_N^\rho = M_N^0$ as $\lambda = 0$. According to equation (A.7), we also have

$$\begin{aligned} \sup_{\tilde{\mathbf{x}} \in \Omega} \mathbb{E}_N [M_N^\rho - M_{N,\tilde{\mathbf{x}}}^\rho] &\geq \sup_{\tilde{\mathbf{x}} \in \Omega} \mathbb{E}_N [M_N^0 - M_{N,\tilde{\mathbf{x}}}^\rho] \\ &\geq \sup_{\tilde{\mathbf{x}} \in \Omega} \text{EI}(\tilde{\mathbf{x}}|\mathcal{D}) \cdot \text{DPOF}(\tilde{\mathbf{x}}). \end{aligned} \quad (\text{A.9})$$

Therefore, with the same proof as that of Proposition 2.9 [41], for $N \rightarrow \infty$, (A.8) and (A.9) yield $\sup_{\tilde{\mathbf{x}} \in \Omega} \text{EICB}(\tilde{\mathbf{x}}|\mathcal{D}) \rightarrow 0$. From equation (3), it can be further obtained that $\text{DPOF}(\tilde{\mathbf{x}})\sigma_f(\tilde{\mathbf{x}}) \rightarrow 0$. This completes the proof for the first statement.

The second statement is proven in virtue of the global search ability of EI and corresponding dense evaluated solutions in χ if NEB property is met. We complete the proof by providing the following facts: *i*) $\text{DPOF}(\tilde{\mathbf{x}})\sigma_f(\tilde{\mathbf{x}}) \rightarrow 0$ holds from the first statement; *ii*) $\text{DPOF}(\tilde{\mathbf{x}}) \geq \text{POF}(\tilde{\mathbf{x}})$

since $\rho^i \geq 0$; *iii*) the variance of $\text{POF}(\tilde{\mathbf{x}})$ will not go to zero according to its definition [19]; and *iv*) $\sigma_f(z|\mathcal{F}_N) \rightarrow 0$ for all sequences accordingly. Based on these facts, the sequence is almost surely dense in χ if the GP models have NEB property according to Definition 3. As a result, $f_{\mathcal{D}}^*$ from any sequence converges to f_{χ}^* almost surely when $N \rightarrow \infty$. ■

Appendix Section B. Empirical analysis of EICB

B.1 The illustrative example in Figure 1

The synthetic problem considered in Figure 1 is given as:

$$\begin{aligned} & \text{minimize} && \cos(5x) - \sin(x) \sin(2x), \\ & \text{subject to} && \cos(5x) - \sin(x) \sin(2x) \leq 0, \end{aligned} \tag{B.1}$$

where the objective function and constraint function share the same analytical format. The total search space is $\Omega = [0, 10]$, while in the left of Figure 1 only a sub-region $([2.5, 5.0])$ is plotted for brevity. The initial evaluated points in the left of Figure 1 include: 2 feasible points at $[4.25, 4.7]$, and 4 infeasible points $[2.5, 3.7, 4.2, 5.0]$. We further assume that both objective and constraint are fully observable to efficiently reveal the difference from EIC and EICB, while in all other examples and experiments, we consider POCOPs. The GPR models with Matérn 5/2 kernel and constant mean function are used to build the surrogate models.

In the right of Figure 1, we conduct 5 repeated experiments in which 10 solutions are uniformly sampled for initialization. We use consistent random seeds across different acquisition functions to obtain the same initialization. The total budget for optimization is 8. The median and 1/4, 3/4 quantiles of the best observed objective values are plotted.

B.2 Another instance of the exploration function

The presented design of an exploration function in equations (9) and (10) is still conservative compared to the level-set estimation and active learning techniques since it only considers boundaries with high probability. We are going to introduce another exploration function that aims for uncertainty reduction of the global feasible regions. Inspired by [32], this can be achieved by modifying the utility function in equation (9) into

$$\begin{aligned} \text{MUB}^i(\tilde{\mathbf{x}}) &= \max\{\varepsilon(\tilde{\mathbf{x}}) - |\tilde{g}_i(\tilde{\mathbf{x}})|, 0\} \\ &= \begin{cases} \varepsilon(\tilde{\mathbf{x}}) - \tilde{g}_i(\tilde{\mathbf{x}}), & \tilde{g}_i(\tilde{\mathbf{x}}) \in [0, \varepsilon(\tilde{\mathbf{x}})], \\ \varepsilon(\tilde{\mathbf{x}}) + \tilde{g}_i(\tilde{\mathbf{x}}), & \tilde{g}_i(\tilde{\mathbf{x}}) \in [-\varepsilon(\tilde{\mathbf{x}}), 0], \\ 0, & \text{otherwise.} \end{cases} \end{aligned} \tag{B.2}$$

We name it the most uncertain boundary (MUB) to indicate that it reduces the global uncertainty of feasibility sequentially.

Lemma 1. *Given the utility function in equation (B.2), the expectation of MUB (EMUB) over the*

predicted distribution of $\tilde{g}_i(\tilde{\mathbf{x}})$ takes the following form as

$$\begin{aligned}
\text{EMUB}^i(\tilde{\mathbf{x}}) = & \varepsilon(\tilde{\mathbf{x}}) \left(\Phi(g_i^+(\tilde{\mathbf{x}})) - \Phi(g_i^-(\tilde{\mathbf{x}})) \right) \\
& - \sigma_g^i(\tilde{\mathbf{x}}) \left(2\phi(-\bar{g}_i(\tilde{\mathbf{x}})) \right. \\
& \quad \left. - \phi(g_i^+(\tilde{\mathbf{x}})) - \phi(g_i^-(\tilde{\mathbf{x}})) \right) \\
& + \mu_g^i(\tilde{\mathbf{x}}) \left(2\Phi(-\bar{g}_i(\tilde{\mathbf{x}})) \right. \\
& \quad \left. - \Phi(g_i^+(\tilde{\mathbf{x}})) - \Phi(g_i^-(\tilde{\mathbf{x}})) \right), \tag{B.3}
\end{aligned}$$

where $\bar{g}_i(\tilde{\mathbf{x}}) = \mu_g^i(\tilde{\mathbf{x}})/\sigma_g^i(\tilde{\mathbf{x}})$, $g_i^+(\tilde{\mathbf{x}}) = \beta - \mu_g^i(\tilde{\mathbf{x}})/\sigma_g^i(\tilde{\mathbf{x}})$, $g_i^-(\tilde{\mathbf{x}}) = -\beta - \mu_g^i(\tilde{\mathbf{x}})/\sigma_g^i(\tilde{\mathbf{x}})$, Φ and ϕ denote the cumulative distribution function and probability density function of $\mathcal{N}(0, 1)$, respectively.

Proof. Let $\tilde{g}_i(\tilde{\mathbf{x}}) = \mu_g^i(\tilde{\mathbf{x}}) + \sigma_g^i(\tilde{\mathbf{x}})\epsilon$ with $\epsilon \sim \mathcal{N}(0, 1)$. The expectation of the utility function of MUB is derived by

$$\begin{aligned}
& \mathbb{E}_{\tilde{g}_i(\tilde{\mathbf{x}}) \sim \mathcal{N}(\mu_g^i(\tilde{\mathbf{x}}), \sigma_g^i(\tilde{\mathbf{x}}))} [\text{MUB}^i(\tilde{\mathbf{x}})] \\
= & \mathbb{E}_{\epsilon \sim \mathcal{N}(0, 1)} [\text{MUB}^i(\tilde{\mathbf{x}})] \\
= & \int_{\epsilon \geq |\mu_g^i(\tilde{\mathbf{x}}) + \sigma_g^i(\tilde{\mathbf{x}})\epsilon|} (\epsilon - |\mu_g^i(\tilde{\mathbf{x}}) + \sigma_g^i(\tilde{\mathbf{x}})\epsilon|) \phi(\epsilon) d\epsilon \\
= & \int_{\bar{g}_i(\tilde{\mathbf{x}})}^{g_i^+(\tilde{\mathbf{x}})} (\epsilon - \mu_g^i(\tilde{\mathbf{x}}) - \sigma_g^i(\tilde{\mathbf{x}})\epsilon) \phi(\epsilon) d\epsilon \\
& + \int_{g_i^-(\tilde{\mathbf{x}})}^{\bar{g}_i(\tilde{\mathbf{x}})} (\epsilon + \mu_g^i(\tilde{\mathbf{x}}) + \sigma_g^i(\tilde{\mathbf{x}})\epsilon) \phi(\epsilon) d\epsilon \\
= & \varepsilon (\Phi(g_i^+(\tilde{\mathbf{x}})) - \Phi(g_i^-(\tilde{\mathbf{x}}))) \\
& + \mu_g^i(\tilde{\mathbf{x}}) (2\Phi(\bar{g}_i(\tilde{\mathbf{x}})) - \Phi(g_i^+(\tilde{\mathbf{x}})) - \Phi(g_i^-(\tilde{\mathbf{x}}))) \\
& + \sigma_g^i(\tilde{\mathbf{x}}) \left(\int_{g_i^-(\tilde{\mathbf{x}})}^{\bar{g}_i(\tilde{\mathbf{x}})} \epsilon \phi(\epsilon) d\epsilon - \int_{\bar{g}_i^+(\tilde{\mathbf{x}})}^{g_i^-(\tilde{\mathbf{x}})} \epsilon \phi(\epsilon) d\epsilon \right). \tag{B.4}
\end{aligned}$$

Note the following result holds:

$$\int_a^b x \phi(x) dx = \phi(a) - \phi(b). \tag{B.5}$$

Therefore, the equation (B.3) holds. ■

Based on Lemma 1, we propose a new exploration function as follows:

$$\rho^i(\tilde{\mathbf{x}}, \gamma^i) = \frac{\text{EMUB}^i(\tilde{\mathbf{x}})}{\gamma^i}, \tag{B.6}$$

where $\gamma^i > 0$ denotes a scale parameter.

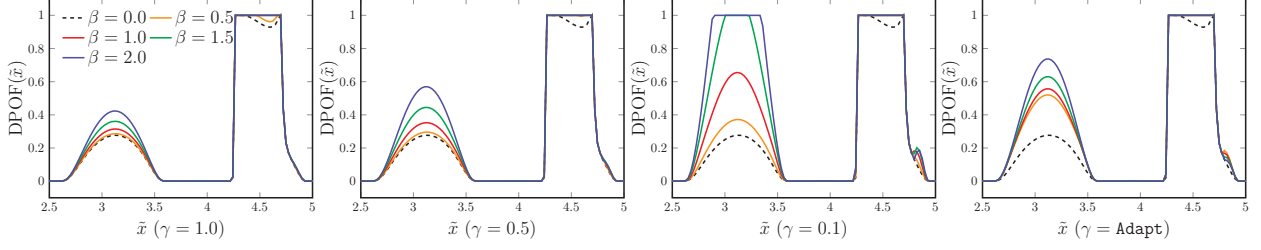


Figure B-1: Illustration of different exploration ability of DPOF with equation (B.3) and different settings of β and γ .

As depicted in Figure B-1, both γ^i and β can effect the exploration ability of equation (B.3). To mitigate the complexity for configuration, we introduce an adaptation law of γ^i as

$$\gamma^i = \text{Adapt}(\tilde{\mathbf{x}}) = \max_{\tilde{\mathbf{x}}} \text{EMUB}^i(\tilde{\mathbf{x}}) \Phi_g^i(\lambda). \quad (\text{B.7})$$

This law enables γ to scale $\text{EMUB}^i(\tilde{\mathbf{x}})$ within $[0, 1]$. As shown in Figure B-1, **Adapt** leads to a more reasonable strategy of weight allocation.

Remark 1. *The dissections to each term in equation (B.3) were made in [26] where the utility function was slightly different from equation (B.2) (they used a squared form as $\varepsilon^2(\tilde{\mathbf{x}}) - \tilde{g}_i^2(\tilde{\mathbf{x}})$ However, the derivation made by [26] was incorrect [27]). In general, the first and third terms in equation (B.3) suggest candidates on the most uncertainty boundaries, while the second term in equation (B.3) suggests candidates from the interior of regions that remain uncertain due to limited observations.*

Remark 2. *The new designed exploration function performs more aggressively, because it explicitly contains the standard deviation σ_g^i that facilitates to reduce the global uncertainty of feasible regions. Unlike the POB and equation (10), EMUB is no longer a conservative design and may assign high weight to a candidate solution that has low POF.*

B.3 Comparative study of EI-based CBO methods

Since we are not interested in calibrating the involved hyperparameters, such as γ^i and β , for better performance in individual problems, we compare three EI-based CBO methods with fixed parameter settings: 1) EIC without hyperparameters, *ii*) EICB-POB using equation (10) with $\beta = 1.96$ (i.e. the 95% confidence level), and *iii*) EICB-MUB using equation (B.6) with $\beta = 1.96$ and γ^i determined by **Adapt**. Note that for EICB-EMUB, β and γ^i are coupled. Despite with **Adapt**, different values of β can still result in distinct optimization trajectories. This is one reason for our recommendation for equation (10) as the exploration function, without paying additional effort on parameter selections.

We conduct four experiments in S1: 5D KBF, 10D KBF, XGB-H and Lunar, as presented in the section of Benchmark suite. The results are shown in Figure B-2. It is observed that, for KBF, EICB-MUB does not outperform EIC. Differently, for XGB-H and Lunar, EICB-MUB is competitive with EICB-POB. Furthermore, it is noticed that the value deviation of EICB-MUB is larger than EICB-POB during optimization processes, which suggests that more exploration is introduced in EICB-MUB. However, this aggressive design can lead to inefficiency for some problems such as KBF

and XGB-H, which is another reason for our preference of using equation (10). Note that we can expect improvements of EICB-MUB by appropriately tuning β and γ^i , which is however out of the scope of this work.

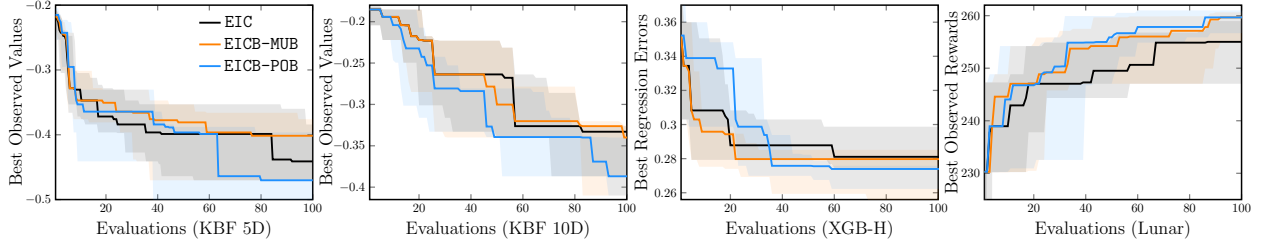


Figure B-2: Optimization trajectories of different tasks using EI-based methods in S1.

Appendix Section C. Expectation Propagation for HLGP

The posterior of the HLGP can be calculated by:

$$p(\tilde{\mathbf{g}}_i|X, \mathbf{g}_i) = \frac{1}{Z} p(\tilde{\mathbf{g}}_i|X) \prod_{k=1}^N p(g_i^k|\tilde{g}_i^k), \quad (\text{C.1})$$

where Z is the normalization factor. For the k -th observation g_i^k , EP assigns it an un-normalized Gaussian distribution $t_i^k \triangleq \tilde{Z}_i^k \mathcal{N}(\tilde{\mu}_i^k, \tilde{\sigma}_i^k{}^2)$ to locally approximate its exact likelihood. In this vein, the posterior is approximated by:

$$p(\tilde{\mathbf{g}}_i|X, \mathbf{g}_i) \approx \frac{1}{Z_{\text{EP}}} p(\tilde{\mathbf{g}}_i|X) \prod_{k=1}^N t_i^k = \mathcal{N}(\boldsymbol{\mu}_g^i, \Sigma_g^i)$$

with $\boldsymbol{\mu}_g^i = \Sigma_g^i \tilde{\Sigma}_g^{i-1} \tilde{\boldsymbol{\mu}}_g^i$ and $\Sigma_g^i = (K + \tilde{\Sigma}_g^{i-1})^{-1}$, (C.2)

where $\tilde{\boldsymbol{\mu}}_g^i = (\tilde{\mu}_i^1, \dots, \tilde{\mu}_i^N)^\top$, $\tilde{\Sigma}_g^i$ denotes a diagonal matrix with the k -th element $\tilde{\sigma}_i^k{}^2$, and Z_{EP} is the marginal likelihood. For HLGP, the site parameters \tilde{Z}_i^k , $\tilde{\mu}_i^k$ and $\tilde{\sigma}_i^k$ in t_i^k are determined by the following laws.

- *Law 1.* The site parameters of an exact Gaussian likelihood $\mathcal{N}(g_i(\mathbf{x}^k), \sigma^2)$ are directly assigned by

$$\tilde{Z}_i^k = 1, \quad \tilde{\mu}_i^k = g_i(\mathbf{x}^k), \quad \tilde{\sigma}_i^k = \sigma. \quad (\text{C.3})$$

- *Law 2.* The site parameters of a non-Gaussian likelihood are computed by the moment match [33]. First, the marginal for \tilde{g}_i^k from (C.2) is $\mathcal{N}(\bar{\mu}_k^i, \bar{\sigma}_k^i{}^2)$, where $\bar{\mu}_k^i$ and $\bar{\sigma}_k^i{}^2$ denote the i -th element of $\boldsymbol{\mu}_g^i$ and i -th diagonal element of Σ_g^i . Then, the cavity parameters, $\bar{\mu}_{-k}^i$ and $\bar{\sigma}_{-k}^i{}^2$, can be computed by

$$\begin{aligned} \bar{\mu}_{-k}^i &= \bar{\sigma}_{-k}^i{}^2 \left(\bar{\sigma}_k^i{}^{-2} \bar{\mu}_k^i - \tilde{\mu}_i^k \tilde{\sigma}_i^k{}^{-2} \right), \\ \bar{\sigma}_{-k}^i{}^2 &= \left(\bar{\sigma}_k^i{}^{-2} - \tilde{\sigma}_i^k{}^{-2} \right)^{-1}. \end{aligned} \quad (\text{C.4})$$

The desired moments on the true likelihood are:

$$\begin{aligned}\hat{\mu}_i^k &= \bar{\mu}_{-k}^i + \frac{\bar{\sigma}_{-k}^{i,2} \phi(z_i^k)}{\Phi(z_i^k) \sqrt{\alpha^2 + \bar{\sigma}_{-k}^{i,2}}}, \\ \hat{\sigma}_i^{k,2} &= \sigma_{-i}^{k,2} - \frac{\bar{\sigma}_{-k}^{i,4} \phi(z_i^k)}{(\alpha^2 + \bar{\sigma}_{-k}^{i,2}) \Phi(z_i^k)} \left(z_i^k + \frac{\phi(z_i^k)}{\Phi(z_i^k)} \right), \\ \hat{Z}_i^k &= \Phi(z_i^k),\end{aligned}\tag{C.5}$$

where $z_i^k = \frac{\bar{\mu}_{-k}^i}{\sqrt{\alpha^2 + \bar{\sigma}_{-k}^{i,2}}}$. Henceforth, the site parameters can be computed by matching the above moments. Mathematically, it means

$$\begin{aligned}\tilde{\mu}_i^k &= \tilde{\sigma}_i^{k,2} \left(\hat{\sigma}_i^{k,2} \hat{\mu}_i^k - \sigma_{-i}^{k,2} \mu_{-i}^k \right), \\ \tilde{\sigma}_i^{k,2} &= \left(\hat{\sigma}_i^{k,2} - \sigma_{-i}^{k,2} \right)^{-1}.\end{aligned}\tag{C.6}$$

As the un-normalized term \tilde{Z}_i^k does not affect the modeling result, we omit its computation here. Detailed derivation of above processes is referred to [29, 33].

- *Law 3.* Repeatedly compute the above two laws for $k = 1, \dots, N$, until all values of the site parameters converge.

Remark 3. *Computational instability and invalid operation may occur when updating the above parameters. We suggest several ways to alleviate this phenomenon. The first way is using calculation tricks with stronger numerical stability, refer to [29] for practical implementation of an EP algorithm. When non-singularity exists, one can fix the covariance matrices by manipulating the eigenvalues, see the implementation of [1]. Moreover, alternative choices of the Non-Gaussian likelihoods, e.g. step function studied in [3], may be more elegant for a description of the truncated distribution.*

Appendix Section D. Experiment Settings

D.1 Algorithm Implementation

CBO methods

We use GpflowOpt to implement all the algorithms, where the EIC algorithm has been officially presented therein [43]. The implementations of TSC⁴ [18] and MESC⁵ [13] are planted from their official open-source projects. For MESC, we choose to use 20 samples with a 1000 grid in Thompson sampling. For TSC, we fix the grid number as 1000. In our experiments, for higher number of samples and grids, we did not observe significant improvements. For CBOB, we fix $\beta = 1.96$ for 95% confidence level. Note that tuning β will not leads to significant different behaviors of CBOB with the conservative exploration function designed in equation (10).

⁴<https://github.com/pytorch/botorch>

⁵<https://github.com/takeuchi-lab/CMES-IBO>

Gaussian processes

Uniformly, the GPR models are used to build the surrogate models of objective functions, where observations are sequentially obtained with a mask on infeasible solutions. We use GPR, GPC, and HLGP models to build models of constraints for specific algorithms and tasks. All GP models take a constant mean function and the Matérn 5/2 kernel. The GPC models are created by the default builder of Gpflow with initial observations [43], and optimized by the variational inference. For HLGPs, we first modify the raw observations using the EP algorithm in consideration of different likelihood functions. Then the GP model with heterogeneous noises is utilized, referring to the user manual of Gpflow⁶.

More configurations

All acquisition functions are optimized by the L-BFGS-B method with 1000 iterations. The hyper-parameters in all GP models are optimized according to the batch optimizer embedded in GPflow. All illustrative examples and experiments are performed on a desktop with Intel(R) Xeon(R) CPU E5-2620 v4 (2.10GHz) and NVIDIA GeForce GTX 1080Ti GPU.

D.2 Synthetic Benchmark

KBF

The Keane bump function (KBF) is a synthetic constrained optimization problem for testing constrained optimization methods [35]. It consists of one objective function and two constraint functions. We consider the 10D KBF with the search space as $[0, 10]^{10}$.

Ackley

This problem is studied in [18]. The Ackley function is used with the recommended variable values⁷. The single constraint considered in this problem is $\sum_{i=1}^{10} x_i \leq 0$. Besides, the search space is given by $[-5.0, 5.0]^{10}$, and the optimum is located at the origin of the axes such that $f(\vec{0}) = 0$.

WBD

The standard definition of the welded beam design problem is given in [36]. We use the search space $x_1, x_4 \in [0.125, 5]$ and $x_2, x_3 \in [0.1, 10]$, which is also used in [38]. EIC finds a good solution within 20 FEs, but will be stagnated in the following evaluations. Differently, CBOB has less efficiency in the early stage, but can gradually find a good solution without prolonged stagnation.

PVD

The standard definition of the pressure vessel design problem can be found in [38]. The search space is adopted from [18] as $x_1 \in [0, 20]$, $x_2 \in [0, 20]$, $x_3 \in [10, 50]$ and $x_4 \in [150, 200]$. To deal with the discrete variable x_1 and x_2 , we uniformly round them to be integers. In this experiment, MES_c fails to find a better solution within 100 function evaluations, therefore omitted in its results.

⁶<https://gpflow.github.io/GPflow>

⁷<https://www.sfu.ca/~ssurjano/ackley.html>

D.3 Real-World Benchmark

We consider two kinds of real-world problems, i.e., the hyperparameter optimization (HPO) for a good machine learning model and the reinforcement learning for a better controller. Therein, we consider the model size and energy consumption as the analytically unknown constraints. The constraint thresholds are determined by the mean values of the model size or total energy after 2000 repetitive experiments with randomly sampled solutions. Therefore, about 50% solutions of the initial evaluations are infeasible.

XGB-H

The California housing is a regression problem with 20640 samples. The dataset is prepared with a 0.25 train/test split in scikit-learn. The XGBoost regressor⁸ is used to fit the dataset, for which we optimize 7 configurable parameters with different algorithms. The parameters include: learning rate $[2^{-10}, 1]$ (log), maximum depth $[1, 15]$ (Int), subsample ratio of columns $[0.01, 1]$, L2 regularization term $[2^{-10}, 2^{10}]$ (log), L1 regularization term $[2^{-10}, 2^{10}]$ (log), minimum sum of instance weight in a child $[1, 2^7]$ (log), and number of estimators $[1, 2^8]$ (log, Int). We round the solutions for integer parameters. With 2000 repetitive experiments, the model size threshold is 50000bytes.

MLP-D

The digits dataset contains 1797 images of handwriting digits from 1-10. It is a common classification problem and prepared with a 0.25 train/test split in scikit-learn. We use Multi-layer Perceptron (MLP) classifier to fit the dataset, for which we optimize 8 configurable parameters with different algorithms. The parameters include: two sizes of the hidden layers $[2^2, 2^8]^2$ (log, Int), batch size $[2^2, 2^8]$ (log, Int), L2 regularization term $[10^{-8}, 10^{-3}]$ (log), initial learning rate $[10^{-5}, 1]$ (log), tolerance for the optimization $[10^{-6}, 10^{-2}]$ (log), two exponential decay rates in Adam $[0, 0.9999]^2$. With 2000 repetitive experiments, the model size threshold is 107000bytes.

Lunar

In this experiment, we should design a controller that renders a rocket to land on the target position with more reward determined by *i*) the distance to the target, *ii*) fuel consumption, and *iii*) whether crashed. As studied in [37], a heuristic controller with 12 parameters can be designed to control the rocket. We use 'LunarLander-v2' in simulations, where the fuel consumption is separated as an energy constraint. In this task, the fuel consumption should be less than 40.0. The search space is $[0, 2]^{12}$. To create a deterministic environment, we fix the terrain and initial state of the rocket.

Swimmer

In this experiment, the goal is to control a swimmer to move as fast as possible towards one direction. In the MuJoCo environment [44], we use 'swimmer-v4' which contains 8D output state space and 2D action space. As designed in [39], the linear feedback controller is utilized, resulting in 16 parameters in the control gain matrix to be determined. Similarly, we separate the control cost, which was considered in the total reward, as an energy constraint. The constraint threshold

⁸<https://github.com/dmlc/xgboost/>

is set as 1.2. The search space is set as $[-1, 1]^{16}$. To obtain a robust controller against small noises, in each evaluation, the simulation runs 5 times with different initialization seeds.

Appendix Section E. Further Discussions

E.1 Limitations

Our investigations of EICB have two limitations. First, we only study the asymptotic convergence of EICB, from which we cannot give definite answers on whether EICB outperforms EIC at the convergence rate in theory. On the other hand, the empirical design of exploration functions needs to be further studied for a better guidance to the practitioners.

In addition to EICB, the design of HLGP models can be further improved in consideration of the uncertainty on observed solutions. Specifically, the HLGP in its current form cannot eliminate the uncertainty on an evaluated infeasible point, as depicted in Figure 2 of our manuscript. Note that GPC also fails to eliminate the uncertainty. Differently, a classifier such as SVM or MLP with appropriate model capacity can easily achieve this goal. We believe a more complex design of the surrogate models can be leveraged to better exploit the mixed observations.

E.2 Potential Impact

The proposed DPOF is a new constraint handling technique that can be easily integrated to non-negative acquisition functions, such as EI, probability of improvement, parzen estimator, and density-ratio estimation. With other acquisition functions, the theoretical analysis on both convergence and regret bound may be conducted, potentially leading to a more principled design of DPOF. Besides, our work gives criteria for the research focusing on the adaptive design of CBO methods by leveraging information from similar tasks for better optimization with unknown constraints.

References

- [1] A. Marco, D. Baumann, M. Khadiv, P. Hennig, L. Righetti, and S. Trimpe, “Robot learning with crash constraints,” *IEEE Robotics Autom. Lett.*, vol. 6, no. 2, pp. 1439–1446, 2021.
- [2] V. Perrone, I. Shcherbatyi, R. Jenatton, C. Archambeau, and M. W. Seeger, “Constrained bayesian optimization with max-value entropy search,” *CoRR*, vol. abs/1910.07003, 2019. [Online]. Available: <http://arxiv.org/abs/1910.07003>
- [3] R. Garnett, *Bayesian Optimization*. Cambridge University Press, 2023.
- [4] D. V. Lindberg and H. K. Lee, “Optimization under constraints by applying an asymmetric entropy measure,” *J. Comput. Graph. Stat.*, vol. 24, no. 2, pp. 379–393, 2015.
- [5] G. Brockman, V. Cheung, L. Pettersson, J. Schneider, J. Schulman, J. Tang, and W. Zaremba, “Openai gym,” 2016.
- [6] M. Schonlau, W. J. Welch, and D. R. Jones, *Global Versus Local Search in Constrained Optimization of Computer Models*. Institute of Mathematical Statistics, 1 1998, vol. 34, pp. 11–25.

- [7] J. R. Gardner, M. J. Kusner, Z. E. Xu, K. Q. Weinberger, and J. P. Cunningham, “Bayesian optimization with inequality constraints,” in *ICML’14: Proc. of the 31th International Conference on Machine Learning*, vol. 32. JMLR.org, 2014, pp. 937–945.
- [8] M. A. Gelbart, J. Snoek, and R. P. Adams, “Bayesian optimization with unknown constraints,” in *UAI’14: Proc. of the 13th Conference on Uncertainty in Artificial Intelligence*. AUAI Press, 2014, pp. 250–259.
- [9] B. Letham, B. Karrer, G. Ottoni, and E. Bakshy, “Constrained bayesian optimization with noisy experiments,” *Bayesian Anal.*, vol. 14, no. 2, pp. 495 – 519, 2019.
- [10] R. Lam and K. Willcox, “Lookahead bayesian optimization with inequality constraints,” in *NeurIPS’17: Annual Conference on Neural Information Processing Systems*, 2017, pp. 1890–1900.
- [11] Y. Zhang, X. Zhang, and P. I. Frazier, “Two-step lookahead bayesian optimization with inequality constraints,” in *NeurIPS’21: Annual Conference on Neural Information Processing Systems*, 2021, pp. 12 563–12 575.
- [12] J. M. Hernández-Lobato, M. A. Gelbart, M. W. Hoffman, R. P. Adams, and Z. Ghahramani, “Predictive entropy search for bayesian optimization with unknown constraints,” in *ICML’15: Proc. of the 32nd International Conference on Machine Learning 2015*, vol. 37. JMLR.org, 2015, pp. 1699–1707.
- [13] S. Takeno, T. Tamura, K. Shitara, and M. Karasuyama, “Sequential and parallel constrained max-value entropy search via information lower bound,” in *ICML’22, Proc. of the 39th International Conference on Machine Learning*, vol. 162. PMLR, 2022, pp. 20 960–20 986.
- [14] S. Belakaria, A. Deshwal, and J. R. Doppa, “Max-value entropy search for multi-objective bayesian optimization,” in *NeurIPS’19: Annual Conference on Neural Information Processing Systems*, 2019, pp. 7823–7833.
- [15] R. B. Gramacy, G. A. Gray, S. L. Digabel, H. K. H. Lee, P. Ranjan, G. N. Wells, and S. M. Wild, “Modeling an augmented lagrangian for black-box constrained optimization,” *Technometrics*, vol. 58, no. 1, pp. 1–11, 2016.
- [16] V. Picheny, R. B. Gramacy, S. M. Wild, and S. L. Digabel, “Bayesian optimization under mixed constraints with a slack-variable augmented lagrangian,” in *NeurIPS’16: Annual Conference on Neural Information Processing Systems*, 2016, pp. 1435–1443.
- [17] S. Ariaifar, J. Coll-Font, D. H. Brooks, and J. G. Dy, “ADMMBO: bayesian optimization with unknown constraints using ADMM,” *J. Mach. Learn. Res.*, vol. 20, pp. 123:1–123:26, 2019.
- [18] D. Eriksson and M. Poloczek, “Scalable constrained bayesian optimization,” in *AISTATS’21: Proc. of the 24th International Conference on Artificial Intelligence and Statistics*, vol. 130. PMLR, 2021, pp. 730–738.
- [19] F. Bachoc, C. Helbert, and V. Picheny, “Gaussian process optimization with failures: Classification and convergence proof,” *J. Glob. Optim.*, vol. 78, no. 3, pp. 483–506, 2020.

- [20] A. Candelieri, “Sequential model based optimization of partially defined functions under unknown constraints,” *J. Glob. Optim.*, vol. 79, no. 2, pp. 281–303, 2021.
- [21] T. Pourmohamad and H. K. H. Lee, “Multivariate stochastic process models for correlated responses of mixed type,” *Bayesian Anal.*, vol. 11, pp. 797 – 820, 2016.
- [22] Y. Zhang, Z. Dai, and B. K. H. Low, “Bayesian optimization with binary auxiliary information,” in *UAI’19: Proc. of the 35th Conference on Uncertainty in Artificial Intelligence*, vol. 115. AUAI Press, 2019, pp. 1222–1232.
- [23] J. M. Parr, A. J. Keane, A. I. Forrester, and C. M. Holden, “Infill sampling criteria for surrogate-based optimization with constraint handling,” *Eng. Optim.*, vol. 44, no. 10, pp. 1147–1166, 2012.
- [24] V. Picheny, “A stepwise uncertainty reduction approach to constrained global optimization,” in *AISTATS’14: Proc. of the 17th International Conference on Artificial Intelligence and Statistics*, vol. 33. JMLR.org, 2014, pp. 787–795.
- [25] Z. Wang and M. Ierapetritou, “Constrained optimization of black-box stochastic systems using a novel feasibility enhanced kriging-based method,” *Comput. Chem. Eng.*, vol. 118, pp. 210–223, 2018.
- [26] P. Ranjan, D. Bingham, and G. Michailidis, “Sequential experiment design for contour estimation from complex computer codes,” *Technometrics*, vol. 50, no. 4, pp. 527–541, 2008.
- [27] J. Bect, D. Ginsbourger, L. Li, V. Picheny, and E. Vázquez, “Sequential design of computer experiments for the estimation of a probability of failure,” *Stat. Comput.*, vol. 22, no. 3, pp. 773–793, 2012.
- [28] F. Bachoc, T. Cesari, and S. Gerchinovitz, “The sample complexity of level set approximation,” in *AISTATS’21: Proc. of the 24th International Conference on Artificial Intelligence and Statistics*, vol. 130. PMLR, 2021, pp. 424–432.
- [29] C. E. Rasmussen and C. K. I. Williams, *Gaussian Processes for Machine Learning*. The MIT Press, 11 2005.
- [30] D. R. Jones, M. Schonlau, and W. J. Welch, “Efficient global optimization of expensive black-box functions,” *J. Glob. Optim.*, vol. 13, no. 4, pp. 455–492, 1998.
- [31] E. Vazquez and J. Bect, “Convergence properties of the expected improvement algorithm with fixed mean and covariance functions,” *J. Stat. Plan. Inference*, vol. 140, no. 11, pp. 3088–3095, 2010.
- [32] B. J. Bichon, M. S. Eldred, L. P. Swiler, S. Mahadevan, and J. M. McFarland, “Efficient global reliability analysis for nonlinear implicit performance functions,” *AIAA J.*, vol. 46, no. 10, pp. 2459–2468, 2008.
- [33] J. Riihimäki and A. Vehtari, “Gaussian processes with monotonicity information,” in *AISTATS’10: Proc. of the 13th International Conference on Artificial Intelligence and Statistics*. JMLR.org, 2010, pp. 645–652.

- [34] T. P. Minka, “Expectation propagation for approximate bayesian inference,” in *UAI '01: Proc. of the 17th Conference in Uncertainty in Artificial Intelligence*. Morgan Kaufmann, 2001, pp. 362–369.
- [35] A. J. Keane, “Experiences with optimizers in structural design,” in *Proc. of the conference on adaptive computing in engineering design and control*, vol. 94, 1994, pp. 14–27.
- [36] K. Deb, “An efficient constraint handling method for genetic algorithms,” *Computer Methods in Applied Mechanics and Engineering*, vol. 186, no. 2, pp. 311–338, 2000.
- [37] D. Eriksson, M. Pearce, J. R. Gardner, R. Turner, and M. Poloczek, “Scalable global optimization via local bayesian optimization,” in *NeurIPS'19: Annual Conference on Neural Information Processing Systems*, 2019, pp. 5497–5508.
- [38] C. A. C. Coello and E. Mezura-Montes, “Constraint-handling in genetic algorithms through the use of dominance-based tournament selection,” *Adv. Eng. Informatics*, vol. 16, no. 3, pp. 193–203, 2002.
- [39] L. Wang, R. Fonseca, and Y. Tian, “Learning search space partition for black-box optimization using monte carlo tree search,” in *NeurIPS'20: Annual Conference on Neural Information Processing Systems*, 2020.
- [40] S. Watanabe and F. Hutter, “c-tpe: Generalizing tree-structured parzen estimator with inequality constraints for continuous and categorical hyperparameter optimization,” in *IJCAI'23: Proc. of the 32th International Joint Conference on Artificial Intelligence*. ijcai.org, 2023.
- [41] J. Bect, F. Bachoc, and D. Ginsbourger, “A supermartingale approach to gaussian process based sequential design of experiments,” *Bernoulli*, vol. 25, no. 4A, pp. 2883–2919, 2019.
- [42] D. Ginsbourger, O. Roustant, and N. Durrande, “On degeneracy and invariances of random fields paths with applications in gaussian process modelling,” *J. Stat. Plan. Inference*, vol. 170, pp. 117–128, 2016.
- [43] A. G. de G. Matthews, M. van der Wilk, T. Nickson, K. Fujii, A. Boukouvalas, P. León-Villagrà, Z. Ghahramani, and J. Hensman, “Gpflow: A gaussian process library using tensorflow,” *J. Mach. Learn. Res.*, vol. 18, pp. 40:1–40:6, 2017.
- [44] E. Todorov, T. Erez, and Y. Tassa, “Mujoco: A physics engine for model-based control,” in *IROS'12: IEEE/RSJ International Conference on Intelligent Robots and Systems*. IEEE, 2012, pp. 5026–5033.